Climate change impacts the vertical structure of marine ecosystem thermal ranges

Yeray Santana-Falcón, Roland Séférian

Climate change impacts the vertical structure of marine ecosystem thermal ranges

Yeray Santana-Falcón*[1] and Roland Séférian[1]

[1]CNRM, Université de Toulouse, Météo-France, CNRS, Toulouse, France

*yeray.santana@meteo.fr

Temperature drives global ocean patterns of biodiversity, shaping thermal niches through thresholds of thermal tolerance. Global warming is predicted to change thermal range bounds, yet research has primarily focused on temperature at the sea surface, while knowledge of changes through the depths of the water column is lacking. Here using daily observations from Ocean Sites and model simulations, we track shifts in ocean temperatures, focusing on the emergence of thermal ranges whose future lower bounds exceed current upper bounds. These emerge below 50 m depth as early as ~2040 with high anthropogenic emissions, yet are delayed several decades for reduced emission scenarios. By 2100, concomitant changes in both lower and upper boundaries can expose pelagic ecosystems to thermal environments never experienced before. These results suggest the redistribution of marine species might differ across depth, highlighting a much more complex picture of the impact of climate change on marine ecosystems.

Anthropogenic climate change impacts the world's oceans by warming significantly the upper layers[1,2]. This heat content increase is projected to alter long-term well defined thermal niches driving species redistribution at a global scale[3,4]. These changes are already affecting goods and services provided by the oceans[5], and are projected to be amplified with rising greenhouse gas emissions. A close coupling between marine organisms' physiological thermal tolerances and environmental temperature[6–9] suggests that distributional shifts can be predicted by tracking changes on the lower and upper bounds of the ecosystems' thermal ranges[10,11]. Since the vertical structure of temperature in the ocean is rarely considered, current understanding on how and when climate change will drive changes in marine habitats is largely restricted to the ocean surface (e.g., ref. [4,12,13]). However, considering only the ocean surface offers a limited view of an ocean under anthropogenic pressure[14], and broad scale studies on how species

distribution will be affected by changes in ecosystems' thermal ranges below the surface are lacking. In this framework, we aim to track the emergence of future changes in marine ecosystem thermal ranges across the water column by following the evolution of the vertical structure of ocean temperature.

Predicting changes in marine ecosystems due to variations in environmental temperature relies on the assumption that species' tolerance ranges reflect the magnitude of local temperature variability[8,15]. Marine organisms tend indeed to live in thermal environments tolerable within their thermal tolerance limits[7,16]. In an attempt to characterize organisms' thermal distribution, Stuart-Smith et al.[10] used the 5th and 95th percentiles range of sea surface temperature. We extend this concept through the water column by considering the lower and upper limits of the thermal range to be represented by the environmental temperature minimum (Tmin) and maximum (Tmax). At each depth, Tmin and Tmax correspond to the annual 1st and 99th percentile as computed using the statistical distribution of daily records, respectively. Since both boundaries are warming or cooling differently across depth in response to climate change, marine organisms will confront transformed thermal environments in the future. In this regard, the level of dissimilarity with environmental conditions at which organisms are adapted to, or climate novelty[17,18], may provide a measure of the range of temperatures never experienced before. The ability of an organism to adapt to this novel thermal environment ultimately depends on the speed at which significant changes emerge[13,19,20]. Therefore, our overarching objective is to understand where, when, and how global warming-induced changes over the water column in the environmental thermal range bounds, i.e., Tmin and Tmax, will take place in the future affecting current marine ecosystems.

We take advantage of comprehensive data sets of daily three-dimensional ocean temperatures from both the long-term Ocean Sites (OS) network and state-of-the-art Earth System Models (ESMs). We select six OS stations for which at least seven years of daily temperature observations from the surface to ~1000 m are available (Supplementary Table 1). We map them into polar, temperate, and tropical domains, and determine the surface area informed by each station by computing the level of similarity in daily temperature profiles using a p-value analysis (Fig. 1a, see Methods). A pattern of alternation of cooling and warming periods is seen over the time of available observations (Fig. 1b). In the two southernmost stations, these episodes predominantly consists on warming periods and last a few years. They last longer in the rest of the stations, at which these episodes end towards general warming. The first 400 m of the water

column at station CIS-1 ends towards general cooling, though warming anomalies dominate during most of the observational period. Though measurements' coverage is not complete along depth and time for some stations, we consider they allow us to confidently compute annual Tmin and Tmax, and extract trends to compare with ESM simulations.

Fifteen-member ensemble simulations were performed with CNRM-ESM2-1[21] (see Methods) encompassing the historical period (1850-2014) followed by three future projections (2015-2100) that explore contrasted emission pathways[22] developed for the sixth Coupled Model Inter-comparison Project[23] (CMIP6); a low (SSP1-2.6), a moderate (SSP2-4.5), and a high (SSP5-8.5) emission pathways. To test the robustness of our results, an ensemble of opportunity consisting of two additional ESMs following a single member SSP5-8.5 simulation is used (see Supplementary Table 2). At each OS location, we extract a subsample of the historical + SSP5-8.5 simulation that matches the observational period. Comparison between both data sets (Extended Data Fig. 1) show simulation deviates from observations at the northernmost stations, especially at station FRAM at which observations show a warming period before 2010 that may originate from an anomaly advection of North Atlantic waters northwards[24]. This anomalous episode can also be behind the positive anomaly at station CIS-1.

Observations and model data are then used to compute profiles of Tmin and Tmax over the observational period. We derive the anomalies of the lower and upper thermal range boundaries by removing the mean temperature profile. These profiles are then employed to determine the magnitude of the thermal range across depth (Fig. 2), informing the vertical structure of current ecosystems' thermal environment. To assess that the vertical structure of the thermal environment is not biased by the short time period of available observations, we additionally compute these profiles for a 30 years subsample of model data at each station. A comparative analysis (see Supplementary Fig. 1) shows that observational period profiles are consistent with longer time span profiles. Thermal ranges decrease toward high and low latitudes[8] being wider at temperate domains, where they average ~5º C across the first 1000 m depth, and toward deeper layers as the temperature interannual variability also declines. The largest amplitude of the thermal range takes place in the first 200 m of the water column (5.8º C on average) where most of the biota lives[25] , while it narrows to below (1.4ºC on average below 200 m).

Environmental thermal ranges can be represented by a combination of their breadth and their midpoint (Fig. 2, middle panels). Thermal breadth corresponds to the difference between Tmin and Tmax. Midpoint temperature (Tmidpoint) is computed as the arithmetic mean of Tmin and

Tmax. Thermal ranges show a wider breadth above 50 m that narrows rapidly with depth. Modelled thermal ranges are in agreement with observed counterparts, except for an underestimation at FRAM. Excluding FRAM, the agreement is further corroborated by Tmidpoint profiles ($R^2 > 0.8$). At MBARI, simulated thermal ranges as well as the Tmidpoint profile are warmer than derived from the observations, maybe due to the difficulties of ESMs to simulate eastern boundary regions as the California upwelling (see ref. [21,26,27]).

Concomitant changes in thermal range boundaries

Concomitant changes in thermal range lower and upper boundaries can be seen as a compound event[28] since they can result in several developments of the thermal range (Extended Data Fig. 2). Profiles of the linear trends of change for Tmin and Tmax following SSP5-8.5 (Fig. 2) show that the paces of change of current thermal ranges differ across depth. In fact, significant trends in Tmin and Tmax over recent years (Extended Data Fig. 3 and 4) may lead to various developments of the thermal ranges as depicted by the observations and as simulated by CNRM-ESM2-1. In general, warming trends are stronger than cooling trends thus resulting in warmer thermal ranges. Overlapping this warming, imbalanced warming of Tmax will result in wider thermal ranges while excess warming of Tmin will shrink the thermal range. As global warming trends are likely to increase[29–31], it is key to understand the time at which these changes may occur, pending on the level of future greenhouse gases emission and associated global warming levels.

Emergence of changes in current thermal ranges

We estimate when and where substantial changes in the thermal ranges may emerge from warming-induced changes in their bounds, by modifying the canonical approach of the Time of Emergence[32] (ToE). We track the evolution of Tmin across the water column under the three contrasted scenarios with respect to the current (1990 to 2020) Tmidpoint and Tmax, considered as key thresholds for marine ecosystems. We also built a 5th-95th confidence interval for each ToE estimate accounting for internal climate variability, by using a distribution of 100 randomly selected 30 yearslong subsamples of the piControl simulation. When Tmin surpasses a first threshold (Tmidpoint), we consider that the shift of the thermal range may represent a *warning* to current ecosystems since Tmidpoint has been observed to align well with the temperature of maximum ecological success (see ref. [9,33]). Furthermore, when an ecosystem will be exposed to a Tmin that is warmer than the current Tmax, we consider that

organisms should deal with a completely *new thermal range* (see Fig. 3a). Since marine organisms are strongly sensitive to changes in their upper boundary (e.g., ref. [34,35]), we combine this analysis with tracking the timing at which the accumulation of heat in the ocean due to ocean warming causes Tmax to exceed current natural variability, a threshold that can be up to 30% higher than current Tmax. Altogether, these metrics provide a comprehensive view on how climate change will transform marine thermal environments.

The earliest times of emergence of Tmax from current natural variability appear before mid-century (Fig. 3b). Consistently across scenarios, warmer Tmax will affect the upper (0 – 50 m) and lower (50 – 200 m) epipelagic waters in the next few decades (firstly appearing from 2022 to 2053, depending on the station), though this warning will occur sooner (as early as during the present decade) in the mesopelagic waters (200 – 1000 m) of all stations. Tmax-based times of emergence delay up to several decades when moderate and low emission scenarios are considered. However, this feature is less consistent at mesopelagic waters, where early emergence times are relatively independent from the scenario considered, possibly arising from warming commitment due to past emissions or to natural features of the ocean interior (see ref. [36,37]).

For Tmin-based times of emergence, we find a rather good agreement across all stations in the first 200 m of the water column (Fig. 3b), with most Tmin-driven changes in the thermal range appearing within lower epipelagic waters (50 – 200 m). This feature, broadly simulated by the three ESMs (see Supplementary Fig. 2), results from both the shape of current thermal ranges, and the rather homogeneous pattern of higher warming of Tmax over Tmin in these layers (Fig. 2). In the four northernmost stations, the emergence of these warnings are delayed in the deepest layers (> 700 m) as the rate of change of Tmin decreases with depth, even though current thermal ranges are the narrowest of the vertical profile (see Fig. 2). At BATS, at which Tmin and Tmidpoint are close across the mesopelagic layer, Tmin crosses this threshold as early as the present decade. Small rates of change in the thermal ranges preclude this warning to emerge during this century at the mesopelagic layer of HOT-01 (see Extended Data Fig. 5), though they appear by ~2040 below 700 m depth as Tmin warms more rapidly (see Fig. 2).

The emergence of Tmin crossing current Tmax follows a similar profile of that for Tmidpoint, but with a delay of about two to four decades: all domains see emergence before 2080 for depths above 200 m, and before 2070 for depths below 200 m. Appearance occurs sooner in the tropics than in northern stations.

Consistently across all stations, Tmin-based emergence times are delayed by several years when a moderate emission pathway is considered, and by up to decades when a low emission pathway is accounted for. In general, the emergence of Tmin crossing current Tmidpoint occurs earlier for the high emission scenario than the emergence of Tmin crossing current Tmax for the moderate emission scenario, except at FRAM. However, taking into account the internal variability confidence intervals considered here, it is difficult to distinguish between the emergence times informed by different scenarios.

End-of-the-century thermal ranges

Under the high emission scenario, end-of-the-century (2080 to 2100) thermal ranges differ from those estimated over the historical period (1990 to 2014) (Fig. 4 and Extended Data Fig. 6). In general, both the lower and upper bounds will be warmer across the water column. Situations in which end-of-the-century Tmin will be warmer than historical Tmax occur at all stations within either the lower epipelagic or mesopelagic, or in both layers, in agreement with emergence times shown in Fig. 3. The only exceptions are found in the deepest levels of FRAM, and in most parts of the mesopelagic layer of HOT-01, where Tmax and Tmin are predicted to be slightly cooler.

We track novel thermal space at the end of the century using *Climate Novelty* (C_N, see Methods). This metric accounts for the difference between the historical and end-of-the-century period's thermal ranges, and gives insights of the range of temperatures that has never been experienced before for a particular environment. C_N profiles (Fig. 4) show most lower epipelagic and mesopelagic waters' thermal ranges will be >50% novel, consistently with previous studies (see ref. [38] for climate velocity analysis). At HOT-01, C_N of mesopelagic waters indicates relatively low levels of novelty. Nonetheless, this station presents novel thermal ranges at the very deepest waters, in agreement with the emergence of Tmin crossing Tmax warnings (Fig. 3). At the upper epipelagic waters, the level of novelty is lower than 50% at all stations except FRAM, at which C_N is closer to this value. However, while the overall level of novelty experienced in the upper pelagic waters will be less than in the mesopelagic, organisms there already have to deal with large interannual thermal variability, and may be near the upper limits of their tolerance. As such, the emergence of warmer Tmax (Fig. 3) along with the occurrence of short-term extreme events like marine heatwaves[39,40] (MHW) will impact upper waters. In this respect, an analysis on MHW duration and intensity (Extended Data Fig. 7; see Supplementary Text) shows they will last longer (~2.6 days) and be more intense (>0.3ºC) by 2100 at tropical

stations above 200 m considering SSP5-8.5.

Depending on the station and the layer considered, end-of-the-century thermal ranges will be warmer/cooler as a result of comparable warming/cooling of Tmin and Tmax (Fig. 4). They can also be warmer and narrower as a result of quicker warming of Tmin, or warmer and wider by Tmax warming more rapidly than Tmin. Wider thermal ranges will result above 200 m at all stations under a high-emission scenario, with the only exception at CIS-1 due to an excess warming of Tmin below 50 m (Extended Data Fig. 6). Below 200 m, the pace of warming of both bounds are comparable, generating both wide or narrow thermal ranges depending on the station. Both Tmin and Tmax changes as long as C_N profiles remain similar when considering a moderate emission scenario (SSP2-4.5) (Extended Data Fig. 8), but showing lower difference values between end-of-the-century and historical thermal range bounds. Considering a high mitigation scenario (SSP1-2.6), all stations show warming anomalies (Extended Data Fig. 9), except at station CIS-1 where both bounds will generally be cooler than the historical mean. Only developments at stations FRAM and K276 are consistent across all emission scenarios.

Implications of the work

Current research, mainly based on monthly surface data, suggest an expansion of marine ectotherms toward their poleward range boundaries as a response to the warming of the oceans[41–43]. Our work reveals a much more complex picture, demonstrating the added-value of scrutinizing climate change perturbations on ecosystem thermal ranges across the water column with respect to surface data. We find that climate change will generate changes across the water column in the upper and lower thermal range bounds on six OS stations. If anthropogenic emissions continue to rise, we project that the upper bound of thermal ranges will emerge from current natural variability within the present decade, while the lower bound may cross the upper limit of current thermal ranges as early as ~2040 in pelagic waters. These changes can be delayed several decades with immediate emission reduction consistent with a high mitigation scenario, in line with results included in the last IPCC AR6 report[44] , implying marine habitats are committed to change even if reaching net zero emissions by mid-century. In response to ocean warming, thermal ranges will mostly be warmer by 2100. Nonetheless, excess warming of Tmin with respect to Tmax will result in narrower thermal ranges, while excess warming of Tmax with respect to Tmin will result in wider thermal ranges (Extended Data Fig. 10). In the former case, new conditions will defy local adaptation of inhabitant organisms, possibly leading to the loss of ecosystems' habitability if species cannot adjust their

lifecycle to the contraction of their thermal environment. In the latter, possible spread of species from neighbour habitats may generate additional stresses by changing species interaction[4,45], especially at high-latitude stations where the range of tolerable temperature for marine ectotherms are narrow[8], and the warming of temperate waters may increase the abundance of species at their poleward range boundaries[46]. Furthermore, wider thermal ranges may challenge the capacity limits of species already exposed to large interannual thermal variability by the excess warming of current Tmax. In addition, C_N profiles indicate that the thermal environment will be novel at several depth levels below upper layers, suggesting marine organisms living at depth might be impacted before upper waters thermal ranges undergo substantial changes; including the emergence of warmer Tmax that appear sooner in mesopelagic waters.

Assuming organisms are adapted to current environmental conditions, such changes may lead to important rearrangements of marine habitats across latitude and depth[47] in the decades to come. Though the possibility of looking for refuge at depth may exist for some organisms (e.g., [41,48]), vertical rearrangements may be limited by the capacity of the organisms to acclimate to higher hydrostatic pressure[49], by high light requirements (e.g., [50]), or by deeper thermal ranges that are not suitable anymore. Our work indicates that the resilience of polar organisms, which are very sensitive to elevated temperatures[51,52], will be profoundly affected by substantial changes on current thermal ranges (C_N ~ 100% between 100 to 500 m depth) along with variations in the sea ice coverage (e.g., ref. [53]). In tropical regions, where some species live near their physiological limits[54], our results indicate marine organisms living at depth will be challenged sooner, as rapid warming of Tmin in the mesopelagic layer will reduce their thermal environment. The reduced capacity of adaptation to warmer upper thermal boundaries of organisms living at these aseasonal regions[46,55–57] will reinforce their vulnerability in the next decades by the emergence of Tmax from current natural variability. In temperate areas, ectotherms like the *Atlantic Cod* may be affected by a warmer thermal environment above 200 m, where spawning takes place[58] and by changes in the vertical structure of their thermal range that may disrupt their daily vertical migration (e.g., ref. [59]). In addition, extreme events like MHWs are expected to increase (ref. [60] and Extended Data Fig. 7; see Supplementary Text) with devastating effects on marine ecosystems (e.g., ref. [61–63]).

Anthropogenic climate change is pushing marine organisms to adapt to a less-oxygen acidified warmer ocean[64,65]. These climatic impact drivers, along with numbers of anthropogenic stressors like fishing[66], acoustic pollution[67] or plastics[68], and extreme and compound events[69],

exacerbate marine ecosystems degradation. Our results add new insights on the timing of long-term global warming impacts acting throughout the water column, and suggest that future research should consider the three-dimensional extension of the thermal environment of marine organisms in the assessments of climate change impacts.

Acknowledgements This work was supported by the European Union's Horizon 2020 research and innovation program with the TRIATLAS project under the grant agreement No 817578 (Y.S.F. and R.S), the COMFORT project under the grant agreement No 820989 (Y.S.F. and R.S) and the ESM2025 project under the grant agreement No 101003536 (R.S). We thank L. Kwiatkowski, S. Berthet and E. Sánchez for comments on pre-submission drafts of the manuscript.

Author Contributions Y.S.F. and R.S. conceived the study, developed the data sets, performed the computations and wrote the manuscript.

Competing interests The authors declare no competing interests.

Figure captions

Figure 1: Overview of the Ocean Sites (OS) stations. (a) Geographic location and period of the six available long-term OS stations. Colour code indicates how the OS stations are grouped into polar (blue), temperate (green) and tropical (orange) ocean domains. The shading indicates the ocean domains that are informed by each OS station. (b) Depth-time variations of daily ocean temperature anomalies over the observational period from the surface to 1000 m. Anomalies are computed by removing the daily climatological temperature to daily temperature. Red (blue) colours indicate warmer (cooler) daily temperature variations with respect to the daily climatological temperature. Blank space indicates lack of observational data.

Figure 2: Profiles of thermal ranges. Profiles of the lower (bluish) and upper (reddish) thermal range boundaries anomalies relative to temperature mean over the observational period, for both observations (shading) and model (lines). Model profiles are represented with (bold) and without (thin) applying the observational mask in space and time. Dashed lines demarcate the upper epipelagic, lower epipelagic and mesopelagic layers. Middle panels show profiles of thermal ranges' thermal midpoint (line) and breadth (shading) for observations (orange) and

model (grey). At right, profiles of the linear trends from 1990 to 2100 following SSP5-8.5 are given for both thermal range boundaries.

Figure 3: Emergence of climate change signals in thermal ranges. (a) Schematic explaining how the evolution of Tmin and Tmax may result in the emergence of substantial changes in current thermal ranges. (b) Profiles of the timing of when future Tmin is warmer than current Tmidpoint and Tmax. Confidence interval of the emergence of these thresholds is included by accounting for climate variability. Profiles of the timing of when future Tmax exceeds the natural variability of current Tmax are included. Dashed lines demarcate the upper epipelagic, lower epipelagic and mesopelagic layers. Solid, dashed, dotted lines represent SSP5-8.5, SSP2-4.5, SSP1-2.6.

Figure 4: End-of-the-century thermal ranges. Profiles illustrate anomalies for Tmin and Tmax with respect to temperature mean over last years of the historical simulation (1990 to 2014) for historical and end-of-the-century (2080 to 2100) periods, considering SSP5-8.5. Reddish (bluish) shading areas indicate ocean layers where end-of-the-century Tmin and Tmax are warmer (cooler) than the historical period. Dashed lines demarcate the water column into upper epipelagic, lower epipelagic and mesopelagic. Middle panels *Climate Novelty* profiles represent the novel environmental temperatures experienced with respect to the end-of-the-century thermal range. Boxes indicate how changes in both boundaries have reshaped thermal ranges under the three scenarios.

References

1. Barnett, T. P. *et al.* Penetration of human-induced warming into the World's Oceans. *Science (80-.).* **309**, 284–287 (2005).
2. Levitus, S. *et al.* Global ocean heat content 1955-2008 in light of recently revealed instrumentation problems. *Geophys. Res. Lett.* **36**, n/a-n/a (2009).
3. Poloczanska, E. S. *et al.* Global imprint of climate change on marine life. *Nat. Clim. Chang.* **3**, 919–925 (2013).
4. García Molinos, J. *et al.* Climate velocity and the future global redistribution of marine biodiversity. *Nat. Clim. Chang.* **6**, 83–88 (2016).
5. Free, C. M. *et al.* Impacts of historical warming on marine fisheries production. *Science (80-.).* **363**, 979–983 (2019).

6. Hughes, N. F. & Grand, T. C. Physiological ecology meets the ideal-free distribution: Predicting the distribution of size-structured fish populations across temperature gradients. *Environ. Biol. Fishes* **59**, 285–298 (2000).

7. Tittensor, D. P. *et al.* Global patterns and predictors of marine biodiversity across taxa. *Nature* **466**, 1098–1101 (2010).

8. Sunday, J. M., Bates, A. E. & Dulvy, N. K. Global analysis of thermal tolerance and latitude in ectotherms. *Proc. R. Soc. B Biol. Sci.* **278**, 1823–1830 (2011).

9. Waldock, C., Stuart□Smith, R. D., Edgar, G. J., Bird, T. J. & Bates, A. E. The shape of abundance distributions across temperature gradients in reef fishes. *Ecol. Lett.* **22**, 685–696 (2019).

10. Stuart-Smith, R. D., Edgar, G. J. & Bates, A. E. Thermal limits to the geographic distributions of shallow-water marine species. *Nat. Ecol. Evol.* **1**, 1846–1852 (2017).

11. Pinsky, M. L., Worm, B., Fogarty, M. J., Sarmiento, J. L. & Levin, S. A. Marine taxa track local climate velocities. *Science (80-.).* **341**, 1239–1242 (2013).

12. Beaugrand, G., Edwards, M., Raybaud, V., Goberville, E. & Kirby, R. R. Future vulnerability of marine biodiversity compared with contemporary and past changes. *Nat. Clim. Chang.* **5**, 695–701 (2015).

13. Trisos, C. H., Merow, C. & Pigot, A. L. The projected timing of abrupt ecological disruption from climate change. *Nature* **580**, 496–501 (2020).

14. Levin, L. A. & Le Bris, N. The deep ocean under climate change. *Science (80-.).* **350**, 766–768 (2015).

15. Deutsch, C. A. *et al.* Impacts of climate warming on terrestrial ectotherms across latitude. *Proc. Natl. Acad. Sci.* **105**, 6668–6672 (2008).

16. Sunday, J. M., Bates, A. E. & Dulvy, N. K. Thermal tolerance and the global redistribution of animals. *Nat. Clim. Chang.* **2**, 686–690 (2012).

17. Radeloff, V. C. *et al.* The rise of novelty in ecosystems. *Ecol. Appl.* **25**, 2051–2068 (2015).

18. Lotterhos, K. E., Láruson, Á. J. & Jiang, L.-Q. Novel and disappearing climates in the global surface ocean from 1800 to 2100. *Sci. Rep.* **11**, 15535 (2021).

19. Mora, C. *et al.* The projected timing of climate departure from recent variability. *Nature* **502**, 183–187 (2013).

20. Henson, S. A. *et al.* Rapid emergence of climate change in environmental drivers of marine ecosystems. *Nat. Commun.* **8**, 14682 (2017).

21. Séférian, R. *et al.* Evaluation of CNRM Earth System Model, CNRM□ESM2□1: Role of Earth system processes in present□day and future climate. *J. Adv. Model. Earth Syst.*

11, 4182–4227 (2019).

22. Gidden, M. J. *et al.* Global emissions pathways under different socioeconomic scenarios for use in CMIP6: a dataset of harmonized emissions trajectories through the end of the century. *Geosci. Model Dev.* **12**, 1443–1475 (2019).

23. Eyring, V. *et al.* Overview of the Coupled Model Intercomparison Project Phase 6 (CMIP6) experimental design and organization. *Geosci. Model Dev.* **9**, 1937–1958 (2016).

24. Beszczynska-Möller, A., Fahrbach, E., Schauer, U. & Hansen, E. Variability in Atlantic water temperature and transport at the entrance to the Arctic Ocean, 1997–2010. *ICES J. Mar. Sci.* **69**, 852–863 (2012).

25. Sutton, T. T. Vertical ecology of the pelagic ocean: classical patterns and new perspectives. *J. Fish Biol.* **83**, 1508–1527 (2013).

26. Richter, I. Climate model biases in the eastern tropical oceans: causes, impacts and ways forward. *WIREs Clim. Chang.* **6**, 345–358 (2015).

27. Pozo Buil, M. *et al.* A Dynamically downscaled ensemble of future projections for the California Current System. *Front. Mar. Sci.* **8**, (2021).

28. Leonard, M. *et al.* A compound event framework for understanding extreme impacts. *WIREs Clim. Chang.* **5**, 113–128 (2014).

29. Kwiatkowski, L. *et al.* Twenty-first century ocean warming, acidification, deoxygenation, and upper-ocean nutrient and primary production decline from CMIP6 model projections. *Biogeosciences* **17**, 3439–3470 (2020).

30. Bopp, L. *et al.* Multiple stressors of ocean ecosystems in the 21st century: projections with CMIP5 models. *Biogeosciences* **10**, 6225–6245 (2013).

31. Cheng, L., Abraham, J., Hausfather, Z. & Trenberth, K. E. How fast are the oceans warming? *Science (80-.).* **363**, 128–129 (2019).

32. Hawkins, E. & Sutton, R. Time of emergence of climate signals. *Geophys. Res. Lett.* **39**, n/a-n/a (2012).

33. Stuart-Smith, R. D., Edgar, G. J., Barrett, N. S., Kininmonth, S. J. & Bates, A. E. Thermal biases and vulnerability to warming in the world's marine fauna. *Nature* **528**, 88–92 (2015).

34. Filbee-Dexter, K. *et al.* Marine heatwaves and the collapse of marginal North Atlantic kelp forests. *Sci. Rep.* **10**, 13388 (2020).

35. Román-Palacios, C. & Wiens, J. J. Recent responses to climate change reveal the drivers of species extinction and survival. *Proc. Natl. Acad. Sci.* **117**, 4211–4217 (2020).

36. Silvy, Y., Guilyardi, E., Sallée, J.-B. & Durack, P. J. Human-induced changes to the global

ocean water masses and their time of emergence. *Nat. Clim. Chang.* **10**, 1030–1036 (2020).

37. Cheng, L., Zheng, F. & Zhu, J. Distinctive ocean interior changes during the recent warming slowdown. *Sci. Rep.* **5**, 14346 (2015).

38. Brito-Morales, I. *et al.* Climate velocity reveals increasing exposure of deep-ocean biodiversity to future warming. *Nat. Clim. Chang.* **10**, 576–581 (2020).

39. Frölicher, T. L. & Laufkötter, C. Emerging risks from marine heat waves. *Nat. Commun.* **9**, 650 (2018).

40. Oliver, E. C. J. *et al.* Marine Heatwaves. *Ann. Rev. Mar. Sci.* **13**, 313–342 (2021).

41. Perry, A. L., Low, P. J., Ellis, J. R. & Reynolds, J. D. Climate change and distribution shifts in marine fishes. *Science (80-.).* **308**, 1912–1915 (2005).

42. Chaudhary, C., Richardson, A. J., Schoeman, D. S. & Costello, M. J. Global warming is causing a more pronounced dip in marine species richness around the equator. *Proc. Natl. Acad. Sci.* **118**, e2015094118 (2021).

43. Burrows, M. T. *et al.* Ocean community warming responses explained by thermal affinities and temperature gradients. *Nat. Clim. Chang.* **9**, 959–963 (2019).

44. Pörtner, H.-O., Roberts, D.C., Tignor, M., Poloczanska, E.S., Mintenbeck, K., Alegría, A., Craig, M., Langsdorf, S. & Löschke, S. Möller, V. Okem, A. Rama, B. (eds. . IPCC, 2022: Climate Change 2022: Impacts, Adaptation, and Vulnerability. Contribution of Working Group II to the Sixth Assessment Report of the Intergovernmental Panel on Climate Change. (2022).

45. Cahill, A. E. *et al.* How does climate change cause extinction? *Proc. R. Soc. B Biol. Sci.* **280**, 20121890 (2013).

46. Hastings, R. A. *et al.* Climate change drives poleward increases and equatorward declines in marine species. *Curr. Biol.* **30**, 1572-1577.e2 (2020).

47. Jorda, G. *et al.* Ocean warming compresses the three-dimensional habitat of marine life. *Nat. Ecol. Evol.* **4**, 109–114 (2020).

48. Dulvy, N. K. *et al.* Climate change and deepening of the North Sea fish assemblage: a biotic indicator of warming seas. *J. Appl. Ecol.* **45**, 1029–1039 (2008).

49. Thatje, S. Climate warming affects the depth distribution of marine ectotherms. *Mar. Ecol. Prog. Ser.* **660**, 233–240 (2021).

50. Manuel, S. A., Coates, K. A., Kenworthy, W. J. & Fourqurean, J. W. Tropical species at the northern limit of their range: Composition and distribution in Bermuda's benthic habitats in relation to depth and light availability. *Mar. Environ. Res.* **89**, 63–75 (2013).

51. Peck, L. S., Webb, K. E. & Bailey, D. M. Extreme sensitivity of biological function to

temperature in Antarctic marine species. *Funct. Ecol.* **18**, 625–630 (2004).

52. Peck, L. S., Morley, S. A., Richard, J. & Clark, M. S. Acclimation and thermal tolerance in Antarctic marine ectotherms. *J. Exp. Biol.* **217**, 16–22 (2014).

53. Walsh, J. E. Climate of the arctic marine environment. *Ecol. Appl.* **18**, S3–S22 (2008).

54. Storch, D., Menzel, L., Frickenhaus, S. & Pörtner, H.-O. Climate sensitivity across marine domains of life: limits to evolutionary adaptation shape species interactions. *Glob. Chang. Biol.* **20**, 3059–3067 (2014).

55. Araújo, M. B. *et al.* Heat freezes niche evolution. *Ecol. Lett.* **16**, 1206–1219 (2013).

56. Pörtner, H. O., Peck, L. & Somero, G. Thermal limits and adaptation in marine Antarctic ectotherms: an integrative view. *Philos. Trans. R. Soc. B Biol. Sci.* **362**, 2233–2258 (2007).

57. Qu, Y.-F. & Wiens, J. J. Higher temperatures lower rates of physiological and niche evolution. *Proc. R. Soc. B Biol. Sci.* **287**, 20200823 (2020).

58. Cohen, D.M., Inada, T., Iwamoto, T., and Scialabba, N. *FAO species catalogue. Vol. 10. Gadiform fishes of the world (Order Gadiformes). An annotated and illustrated catalogue of cods, hakes, grenadiers and other gadiform fishes known to date. FAO Fish. Synop.* (FAO, 1990).

59. Strand, E. & Huse, G. Vertical migration in adult Atlantic cod (Gadus morhua). *Can. J. Fish. Aquat. Sci.* **64**, 1747–1760 (2007).

60. Frölicher, T. L., Fischer, E. M. & Gruber, N. Marine heatwaves under global warming. *Nature* **560**, 360–364 (2018).

61. Wernberg, T. *et al.* Climate-driven regime shift of a temperate marine ecosystem. *Science (80-.).* **353**, 169–172 (2016).

62. Smale, D. A. *et al.* Marine heatwaves threaten global biodiversity and the provision of ecosystem services. *Nat. Clim. Chang.* **9**, 306–312 (2019).

63. Cheung, W. W. L. & Frölicher, T. L. Marine heatwaves exacerbate climate change impacts for fisheries in the northeast Pacific. *Sci. Rep.* **10**, 6678 (2020).

64. Brierley, A. S. & Kingsford, M. J. Impacts of climate change on marine organisms and ecosystems. *Curr. Biol.* **19**, R602–R614 (2009).

65. Bijma, J., Pörtner, H.-O., Yesson, C. & Rogers, A. D. Climate change and the oceans – What does the future hold? *Mar. Pollut. Bull.* **74**, 495–505 (2013).

66. Jackson, J. B. C. *et al.* Historical overfishing and the recent collapse of coastal ecosystems. *Science (80-.).* **293**, 629–637 (2001).

67. Duarte, C. M. *et al.* The soundscape of the Anthropocene ocean. *Science (80-.).* **371**, eaba4658 (2021).

68. Rochman, C. M. & Hoellein, T. The global odyssey of plastic pollution. *Science (80-.).* **368**, 1184–1185 (2020).

69. Gruber, N., Boyd, P. W., Frölicher, T. L. & Vogt, M. Biogeochemical extremes and compound events in the ocean. *Nature* **600**, 395–407 (2021).

Methods

Ocean Sites observations

The *Ocean Sites* (OS) network constitutes a worldwide effort to monitor ocean parameters through high-quality data extracted from long-term, high-frequency observations at several locations of the World ocean. Six OS stations, listed in Supplementary Table 1, were selected because of the availability of continuous daily measurements of ocean temperature and salinity across the water column for more than seven years, allowing a robust computation of thermal range boundaries (see below). All of the six stations provide data from the surface to about 1000 m depth, that have been resampled daily at each depth, and then interpolated into the vertical grid of CNRM-ESM2-1 (see below).

Observational data is accessible through http://tds0.ifremer.fr/thredds/catalog/CORIOLIS-OCEANSITES-GDAC-OBS/DATA/. Last accessed was in October 2020.

Simulations

This work exploits simulations from a state-of-the-art Earth system model, CNRM-ESM2-1[21], that has been developed by the CNRM-CERFACS climate group for the sixth phase of the Coupled Model Inter-comparison Project (CMIP6[23]). The ocean component of CNRM-ESM2-1 is NEMOv3.6[70], which resolves ocean dynamics on an eORCA1 grid[71] with 75 vertical z-coordinate levels. This grid offers a horizontal resolution of about 1° with a grid refinement up to 0.3° in the tropics.

In this study, we performed five simulations with CNRM-ESM2-1: a 250 year-long pre-industrial control simulation (without anthropogenic forcing) to estimate the model's internal variability; and a historical simulation from 1850 to 2014 followed by three future scenarios from 2015 to 2100, which are used to derive present and future variations in temperature minimum and

maximum. For each simulation, an ensemble of 15 members has been performed in order to account for the influence of the internal variability in the computation of quantiles (see below).

These simulations were produced using the external forcing as recommended by CMIP6 for the pre-industrial state and the historical period. For the future scenarios we used contrasting pathways: a low (SSP1-2.6), moderate (SSP2-4.5), and high (SSP5-8.5) emission pathways as described in ref. [22].

All simulations provide daily outputs from the ocean surface to 4000 m for ocean temperature and salinity as well as oxygen, pH and net primary productivity. Here, we exploit only the first 47 vertical layers for ocean temperature and salinity in order to describe the first 1000 m depth of the water column. Finally, to ensure both observations and model data (historical + SSP5-8.5 simulation) cover exactly the same period, model data was selected to begin and end at the same date as observations.

Two additional ESMs (details on Supplementary Table 3) have been used in the study to assess the robustness of our results. This robustness analysis is based on a simple intercomparison where model properties (thermal range and ToE) are compared between each other using only a single realization for each model.

Model internal variability

As a consequence of the chaotic nature of processes in the Earth systems being simulated (ocean-atmosphere-land-biosphere-cryosphere), one of the main sources of uncertainties in climatic future projections is their internal variability[72]. One way to isolate these uncertainties is to generate an ensemble of model realizations[73]. Here we make use of an ensemble of 15 members in order to minimise the influence of the internal variability in our computation. Each realization sampling different states of the model climate.

Ocean domains informed by Ocean Site stations

Though OS networks are located throughout the World ocean, our selection of OS stations is disproportionately located in the North Atlantic and North Pacific oceans (see Fig. 1 and Supplementary Table 1). To assess how large is the surface area of ocean domains informed by our six selected OS stations, we compute the level of similarity between daily profiles as

provided by observations and the model hindcast over the current period (1990 to 2020) using the statistical approach presented in ref. [74]. This approach compares simultaneously the mean and the daily variations of OS daily profiles with a neighbour grid-point model profile using a Chi-squared-based test. The test consists in comparing the cumulative sum of the Welch's t_z^2 [75] across depth levels to an empirical Chi-squared distribution with 47 degrees of freedom (i.e., the number of depth levels). We use 10,000 random samples of this Chi-squared distribution to estimate the empirical distribution of the Chi-squared law. The distribution is then used to compute an empirical 'integrated' p-value that represents an objective metric to determine how far the two profiles are consistent between each other within the depth interval.

The empirical 'integrated' p-value allows us to quantify the match between profiles. We establish a threshold of 0.90 to consider a profile over a grid-cell consistent with the OS profile. For further analysis, stations were grouped into three ocean domains: polar, temperate and tropical waters.

Estimation of the environmental temperature range boundaries

The working definition of the ecosystem thermal range, or the environmental temperature range that experiences an ecosystem, employed in this work assumes that organisms track changes in environmental temperature[7,11,76], and that the magnitude of the local temperature variability reflect their ranges of temperature tolerance[8,77]. As a consequence, we infer the vertical structure of ecosystem thermal ranges from their lower and upper limits, which are captured by the minimal and maximal environmental temperature across the water column, respectively.

Thanks to high-frequency data, we provide a robust yearly estimate of these bounds using the annual first (p01, Tmin) and last (p99, Tmax) percentiles of both model and observation temperature time-series at each depth level. Though this approach encompasses most of the range of temperature variability, it can yield more pessimistic projections as tolerance ranges can be wider than environmental thermal ranges[15,55], and as ectotherms display some plasticity to adapt to environmental temperatures that challenge their tolerance limits[78,79]. Nonetheless, there is limited capacity of acclimation when long-term heating occurs[80], especially for tropical species[81] and during reproductive stages[82].

In order to minimize the influence of the internal climate variability when comparing model and data results, we estimate model annual percentiles by grouping the 15 ensemble members.

Thus, model percentile for thermal range is derived from a 365*15=5475 sample of daily outputs at each depth.

The breadth of thermal ranges are estimated as the difference between Tmax and Tmin at each depth level. Midpoint temperatures (Tmidpoint) correspond to the arithmetic mean of Tmin and Tmax, thus assuming normality in the distribution of Tmin and Tmax.

Timing of crossing thermal range thresholds

To track future changes in the thermal range boundaries, we employed a method inspired from the well-established Time of Emergence (ToE) approach (see Supplementary Fig. 3 and 4). As for the ToE approach, our method requires estimates of a climate change signal (S). We estimate it using daily model outputs from 1990 to 2100 for an ensemble of 15 realizations from CNRM-ESM2-1 that has been run following historical and low emission SSP1-2.6, moderate emission SSP2-4.5, and high emission SSP5-8.5 pathways. For each pathway, we define S as the smooth spline (four degrees of freedom) of the variation of Tmin during the full simulation. In general, the ToE approach is defined as the first year at which S surpasses twice the standard deviation of the internal climate variability. Here, in contrast, we make use of different thresholds that have a meaning for ecosystem functioning, which represent key characteristics of the thermal range; Tmidpoint and Tmax. These two thresholds are defined as the average of a smooth spline (four degrees of freedom) of the variation of Tmidpoint and Tmax during the past 30 years from today (1990 to 2020); a period considered to be representative of the current period. We consider the emergence of substantial changes in the current range of temperatures that defines the environmental conditions of a given habitat as the time at which the lower boundary of this range (Tmin) crosses in the future the current thresholds (Tmidpoint and Tmax).

We built a 5th-95th confidence interval for each ToE estimate accounting for the influence of the internal climate variability. For that, we generate 100 30-yearslong samples selected randomly from the piControl simulation. Then, we compute the annual Tmax and Tmidpoint for these samples, and remove the annual mean to them. Finally, we compute the 5th and 95th percentiles of the statistical distribution of the 100 random Tmax and Tmidpoint anomaly samples.

We additionally compute the emergence of changes in the upper limit of the current thermal

range, i.e., Tmax. Particularly, we estimate the time at which Tmax crosses in the future a threshold defined as the current (1990 to 2020) upper boundary plus twice the standard deviation of the statistical distribution of the 100 random Tmax anomaly samples from the piControl simulation (see above).

In order to illustrate that emergence times are not an artifact of the current shape of thermal ranges, we computed the trends of both boundaries during the 1990 to 2100 period following the historical + SSP5-8.5 simulation (third subpanels at Fig. 2). We have chosen this period as it represents the range of years for which we compute ToE. The shape of these profiles allow us to confirm that ToEs are the results of both the vertical structure of the thermal ranges, and the evolution of the lower and upper boundaries through time.

For illustration purposes, we illustrate how our approach works for four depth levels of HOT-01 station (Extended Data Fig. 5).

End-of-the-century environmental temperature ranges

End-of-the-century environmental temperature ranges provide a snapshot of the concomitant changes in thermal range boundaries resulting from climate change. We compute the end-of-the-century thermal ranges from daily data over the 2080 to 2100 period. Fig. 4 displays the end-of-the-century thermal range anomalies of both Tmin and Tmax with respect to the mean over 1990 to 2014, corresponding to the last years of the historical simulation. To compare with the historical profiles, we also include their anomalies. At each depth level, we assess the magnitude of the changes between the end-of-the-century and the historical profiles.

As changes in thermal range boundaries can evolve in both directions, and with a different pace, they may result in a re-arrangement of the vertical shape of the thermal range. To track if end-of-the-century thermal ranges are also wider or narrower, we compute the difference between Tmax and Tmin anomalies at each depth level (Extended Data Fig. 6, 8, and 9). If the difference is positive, thermal ranges will be wider, i.e., Tmax warms more rapidly. If the difference is negative, thermal ranges will be narrower, i.e., Tmin warms more rapidly. If differences are < 0.05 ºC (i.e., level of uncertainty informed from the analysis of the internal variability of thermal range profiles in Extended Data Fig. 4), we consider no changes in the shape of thermal ranges will take place, i.e., only shifting toward warming or cooling is

projected. The three emission pathways are displayed in Extended Data Fig. 6, 8, and 9, respectively.

In Fig. 4 we have assigned a colour code for each of these developments. A depiction of these developments is provided in Extended Data Fig. 2.

We track novel thermal space resulting from changes in end-of-the-century thermal ranges that differ from historical period counterparts using *Climate Novelty* (C_N). As in previous approaches (e.g., ref. [17,18]), our metric approach accounts for the level of dissimilarity to baseline conditions. This metric accounts for the difference between the last years of the historical period, i.e., 1990 to 2014, and end-of-the-century thermal ranges at each depth. It takes the space gained/lost by the warming/cooling of Tmax and Tmin, and by the thermal space loss when future Tmin surpasses current Tmax. This metric is expressed as follows:

$$C_N = (\Delta_{max} + \Delta_{min} - \Delta_{mod})/ThBr ;$$

Where Δ_{max} corresponds to the difference between Tmax at the end-of-the-century and at the historical period. Δ_{min} corresponds to the difference between Tmin at the end-of-the-century and at the historical period. Δ_{mod} corresponds to the intersection of thermal space between future and historical thermal ranges, i.e., when end-of-the-century Tmin > historical Tmax. ThBr is the difference between Tmax and Tmin at the end of the century period. Thus, C_N informs of the range of environmental temperatures that has never been experienced before with respect to the thermal range at the end of the century. We express it in the manuscript as a percentage by multiplying by 100.

Data availability Interpolated data presented in the paper can be accessed via Zenodo at https://doi.org/10.5281/zenodo.6940283.

Code availability All code used in the current study is available from the corresponding author upon reasonable request.

Methods-only references

70. Madec, G. *et al. NEMO ocean engine*. https://www.earth-prints.org/handle/2122/13309 (2017) doi:10.5281/zenodo.3248739.

71. Mathiot, P., Jenkins, A., Harris, C. & Madec, G. Explicit representation and parametrised

impacts of under ice shelf seas in the z□- coordinate ocean model NEMO 3.6. *Geosci. Model Dev.* **10**, 2849–2874 (2017).

72. Dai, A. & Bloecker, C. E. Impacts of internal variability on temperature and precipitation trends in large ensemble simulations by two climate models. *Clim. Dyn.* **52**, 289–306 (2019).

73. Deser, C., Phillips, A., Bourdette, V. & Teng, H. Uncertainty in climate change projections: the role of internal variability. *Clim. Dyn.* **38**, 527–546 (2012).

74. Middag, R. *et al.* Intercomparison of dissolved trace elements at the Bermuda Atlantic Time Series station. *Mar. Chem.* **177**, 476–489 (2015).

75. Welch, B. L. The generalization of Student's' problem when several different population variances are involved. *Biometrika* **34**, 28 (1947).

76. Lenoir, J. *et al.* Species better track climate warming in the oceans than on land. *Nat. Ecol. Evol.* **4**, 1044–1059 (2020).

77. Janzen, D. H. Why mountain passes are higher in the Tropics. *Am. Nat.* **101**, 233–249 (1967).

78. Seebacher, F., White, C. R. & Franklin, C. E. Physiological plasticity increases resilience of ectothermic animals to climate change. *Nat. Clim. Chang.* **5**, 61–66 (2015).

79. Hoffmann, A. A. & Sgrò, C. M. Climate change and evolutionary adaptation. *Nature* **470**, 479–485 (2011).

80. Sandblom, E. *et al.* Physiological constraints to climate warming in fish follow principles of plastic floors and concrete ceilings. *Nat. Commun.* **7**, 11447 (2016).

81. Tewksbury, J. J., Huey, R. B. & Deutsch, C. A. Putting the heat on tropical animals. *Science (80-.).* **320**, 1296–1297 (2008).

82. Dahlke, F. T., Wohlrab, S., Butzin, M. & Pörtner, H.-O. Thermal bottlenecks in the life cycle define climate vulnerability of fish. *Science (80-.).* 369, 65–70 (2020).

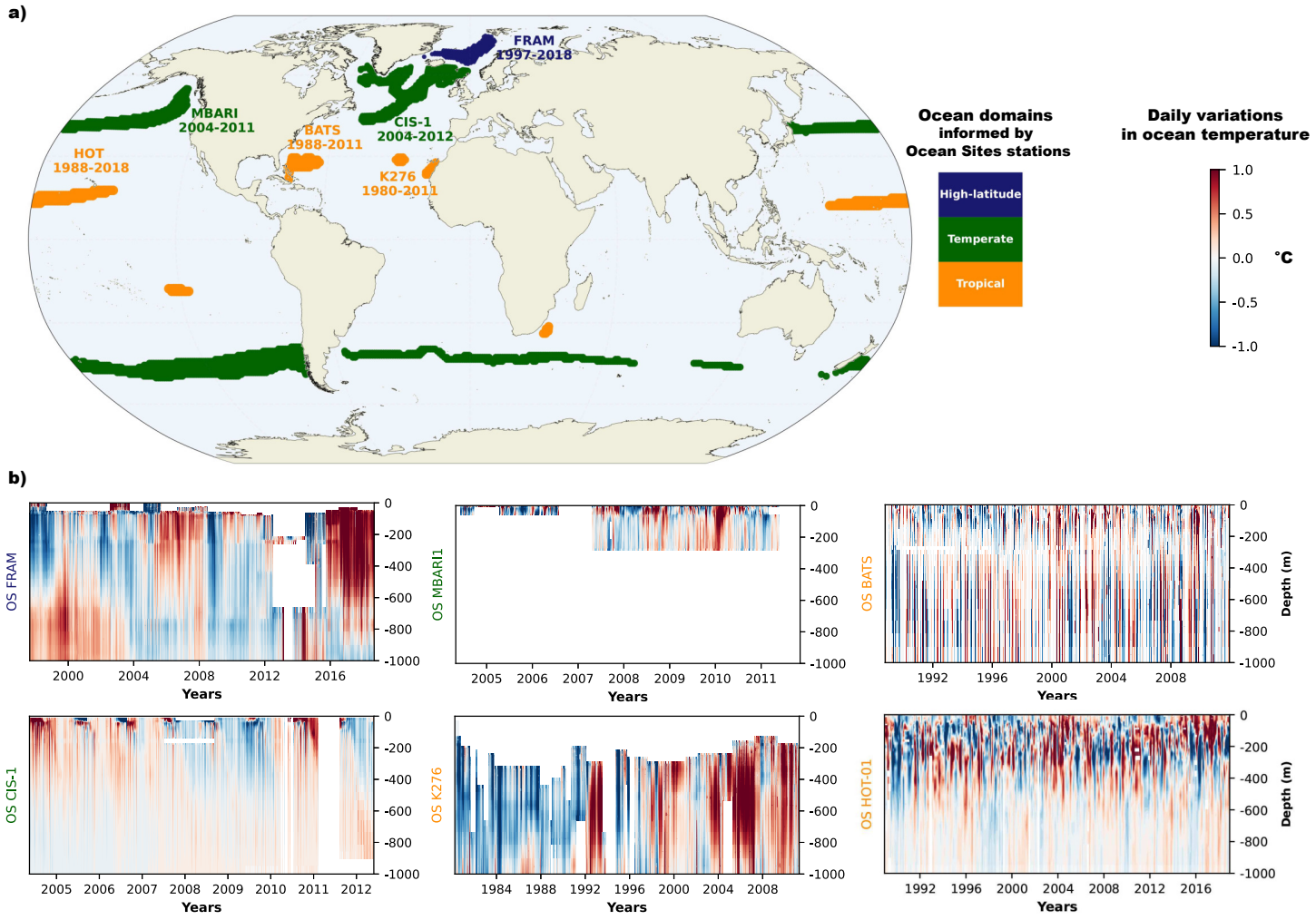
a)
FRAM
1997-2018
MBARI
2004-2011
BATS
1988-2011
CIS-1
2004-2012
HOT
1988-2018
K276
1980-2011
Ocean domains
informed by
Ocean Sites stations
High-latitude
Temperate
Tropical
Daily variations
in ocean temperature
1.0
0.5
0.0
-0.5
-1.0
°C
b)
OS FRAM
OS MBARI1
OS BATS
OS CIS-1
OS K276
OS HOT-01
Depth (m)
Years

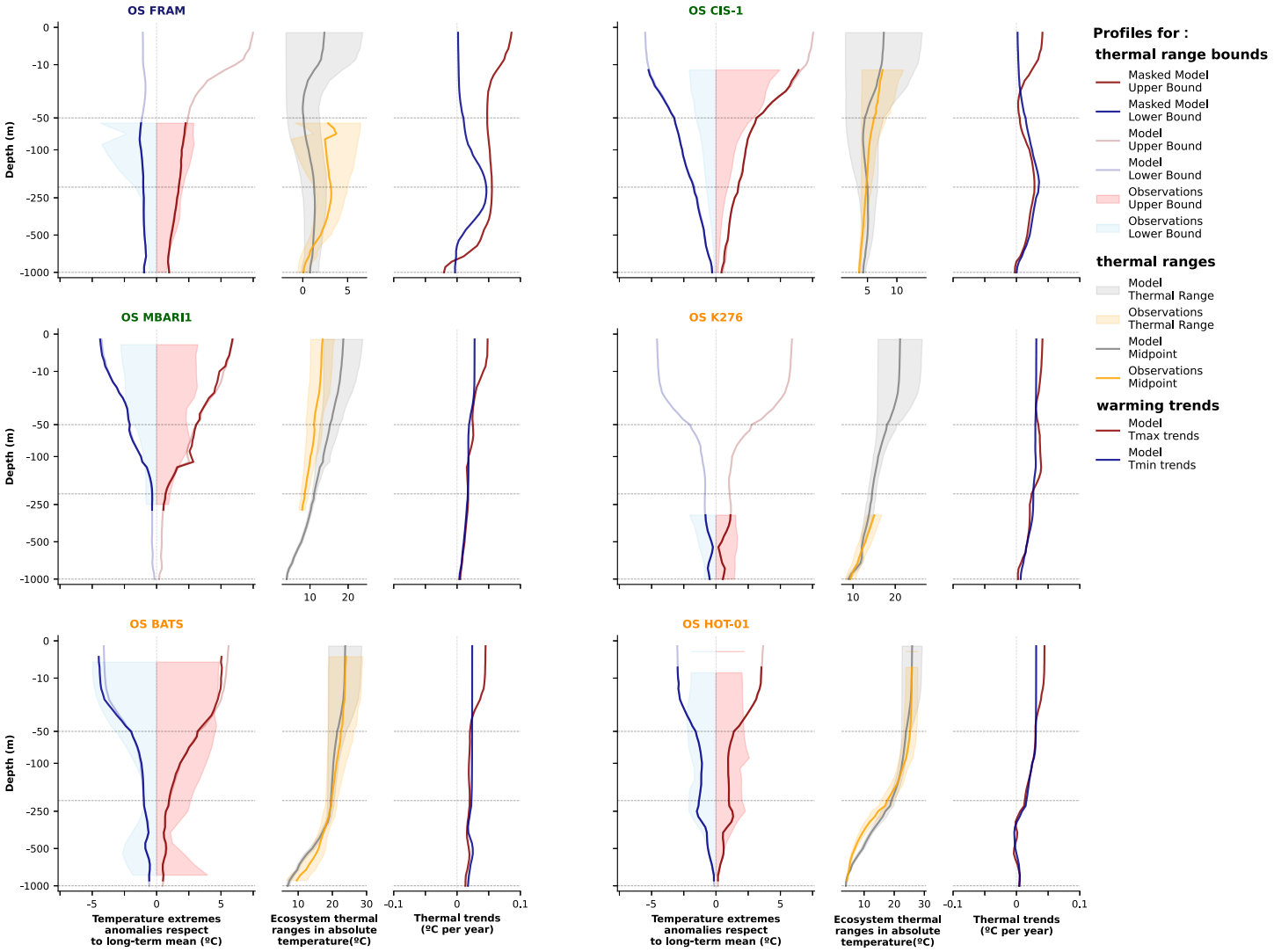
OS FRAM
OS CIS-1
OS MBARI1
OS K276
OS BATS
OS HOT-01
Depth (m)
0
-10
-50
-100
-250
-500
-1000
Profiles for :
thermal range bounds
Masked Model Upper Bound
Masked Model Lower Bound
Model Upper Bound
Model Lower Bound
Observations Upper Bound
Observations Lower Bound
thermal ranges
Model Thermal Range
Observations Thermal Range
Model Midpoint
Observations Midpoint
warming trends
Model Tmax trends
Model Tmin trends
Temperature extremes anomalies respect to long-term mean (ºC)
Ecosystem thermal ranges in absolute temperature(ºC)
Thermal trends (ºC per year)

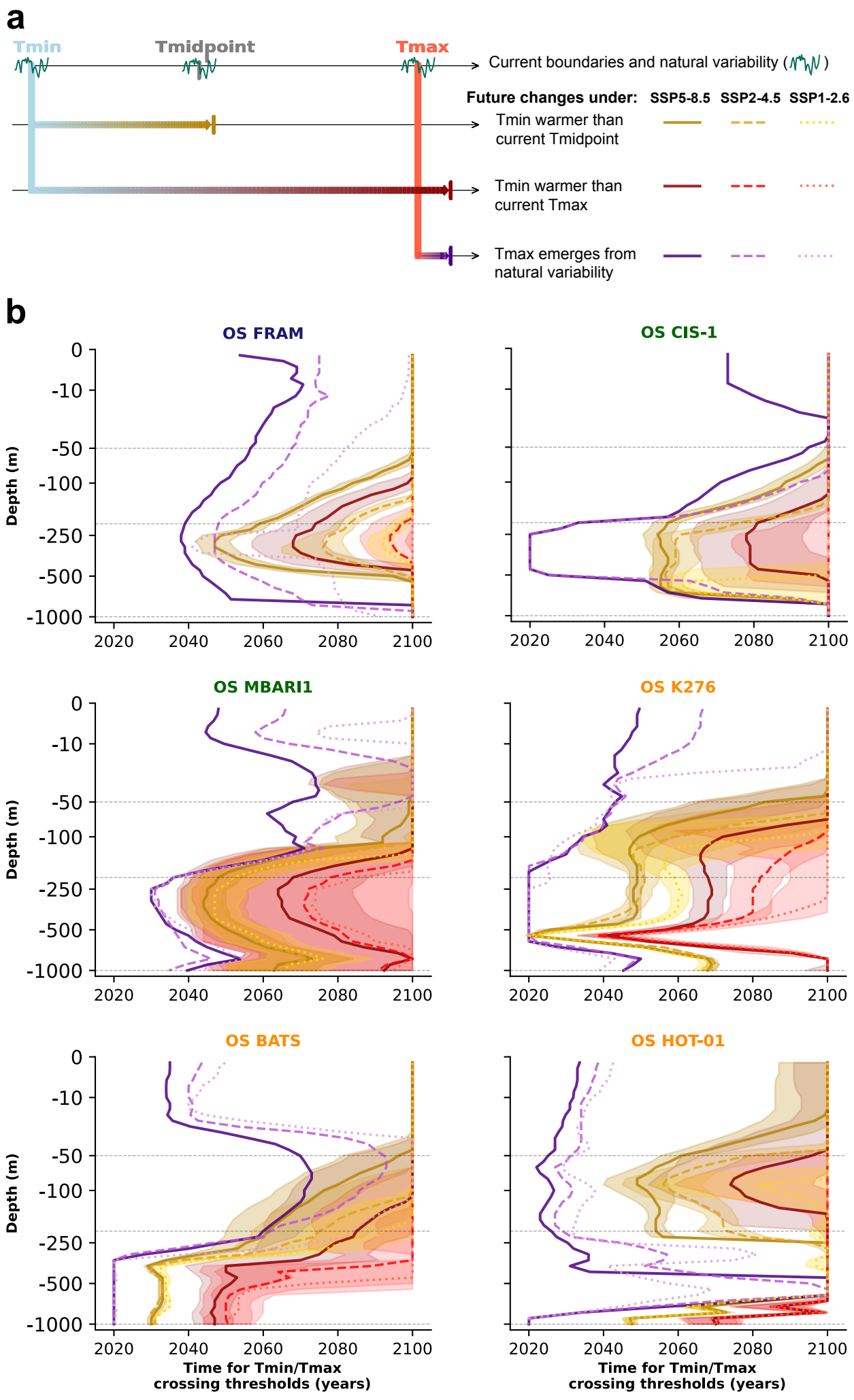
a
Tmin
Tmidpoint
Tmax
Current boundaries and natural variability ( )
Future changes under:
SSP5-8.5
SSP2-4.5
SSP1-2.6
Tmin warmer than current Tmidpoint
Tmin warmer than current Tmax
Tmax emerges from natural variability
b
OS FRAM
OS CIS-1
OS MBARI1
OS K276
OS BATS
OS HOT-01
Depth (m)
0
-10
-50
-100
-250
-500
-1000
2020
2040
2060
2080
2100
Time for Tmin/Tmax crossing thresholds (years)

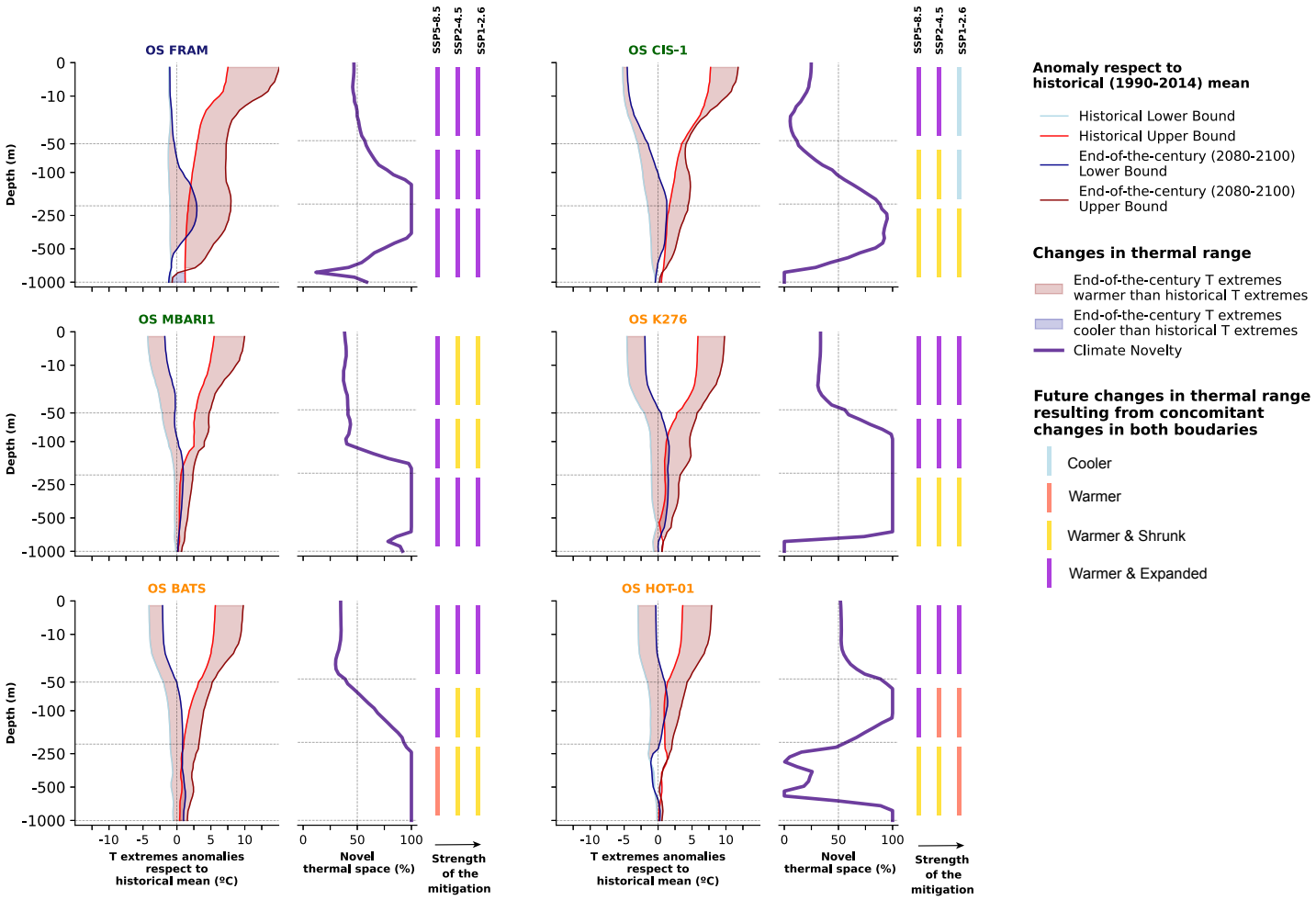
OS FRAM
OS CIS-1
OS MBARI1
OS K276
OS BATS
OS HOT-01
Depth (m)
0
-10
-50
-100
-250
-500
-1000
SSP5-8.5
SSP2-4.5
SSP1-2.6
-10 -5 0 5 10
T extremes anomalies respect to historical mean (ºC)
0 50 100
Novel thermal space (%)
Strength of the mitigation
Anomaly respect to historical (1990-2014) mean
Historical Lower Bound
Historical Upper Bound
End-of-the-century (2080-2100) Lower Bound
End-of-the-century (2080-2100) Upper Bound
Changes in thermal range
End-of-the-century T extremes warmer than historical T extremes
End-of-the-century T extremes cooler than historical T extremes
Climate Novelty
Future changes in thermal range resulting from concomitant changes in both boudaries
Cooler
Warmer
Warmer & Shrunk
Warmer & Expanded